OPEN ACCESS Freely available online

PLoS one

Stabilizing Salt-Bridge Enhances Protein Thermostability by Reducing the Heat Capacity Change of Unfolding

Chi-Ho Chan, Tsz-Ha Yu, Kam-Bo Wong*

School of Life Sciences, Centre for Protein Science and Crystallography, The Chinese University of Hong Kong, Hong Kong, Shatin, Hong Kong SAR, China

Abstract

Most thermophilic proteins tend to have more salt bridges, and achieve higher thermostability by up-shifting and broadening their protein stability curves. While the stabilizing effect of salt-bridge has been extensively studied, experimental data on how salt-bridge influences protein stability curves are scarce. Here, we used double mutant cycles to determine the temperature-dependency of the pair-wise interaction energy and the contribution of salt-bridges to ΔC_p in a thermophilic ribosomal protein L30e. Our results showed that the pair-wise interaction energies for the salt-bridges E6/R92 and E62/K46 were stabilizing and insensitive to temperature changes from 298 to 348 K. On the other hand, the pair-wise interaction energies between the control long-range ion-pair of E90/R92 were negligible. The ΔC_p of all single and double mutants were determined by Gibbs-Helmholtz and Kirchhoff analyses. We showed that the two stabilizing salt-bridges contributed to a reduction of ΔC_p by 0.8–1.0 kJ mol^{-1} K^{-1}. Taken together, our results suggest that the extra salt-bridges found in thermophilic proteins enhance the thermostability of proteins by reducing ΔC_p, leading to the up-shifting and broadening of the protein stability curves.

Citation: Chan C-H, Yu T-H, Wong K-B (2011) Stabilizing Salt-Bridge Enhances Protein Thermostability by Reducing the Heat Capacity Change of Unfolding. PLoS ONE 6(6): e21624. doi:10.1371/journal.pone.0021624

Editor: Annalisa Pastore, National Institute for Medical Research, Medical Research Council, London, United Kingdom

Received April 17, 2011; **Accepted** June 3, 2011; **Published** June 24, 2011

Funding: This work was funded by the General Research Fund of Research Grants Council of Hong Kong (Project no. 476307). The funders had no role in study design, data collection and analysis, decision to publish, or preparation of the manuscript.

Competing Interests: The authors have declared that no competing interests exist.

* E-mail: kbwong@cuhk.edu.hk

Introduction

To survive in the hot habitats, proteins from thermophilic organisms are more thermal stable than their mesophilic homologs. The conformational stability of proteins is defined as the free energy difference between the native and the unfolded states, or the free energy of unfolding (ΔG_u). ΔG_u varies with temperature as a curve function (i.e. the protein stability curve), which is described by the Gibbs-Helmholtz equation:

$$\Delta G_u = \Delta H_m(1 - T/T_m) - \Delta C_p[(T_m - T) + T\ln(T/T_m)]$$

where T_m is the melting temperature, ΔH_m is the enthalpy change of protein unfolding at T_m, and ΔC_p is the heat capacity change of unfolding.

Nojima and co-workers pointed out that protein thermostability, or increase in T_m, can in theory be enhanced by: (i) up-shifting, (ii) broadening, and (iii) right-shifting of the protein stability curves [1]. Nussinov and co-workers studied the correlation between different thermodynamic parameters of 5 protein families and showed that thermophilic proteins prefer to increase T_m by up-shifting and broadening of their protein stability curves [2]. In a later study, Razvi and Scholtz systematically compared the protein stability curves of 26 thermo- and mesophilic homologous pairs of proteins. Regardless to the physical origins, they showed that over 70% of thermophilic proteins in their study achieve higher T_m by up-shifting and/or broadening of their protein stability curves as compared with their mesophilic homologous [3]. It is clear that most thermophilic proteins achieve higher thermostability by up-shifting and broadening of their protein stability curves.

The Gibbs-Helmholtz equation predicts that a smaller ΔC_p can up-shift and broaden a protein stability curve. For example, the curvature of the protein stability can be defined as the second derivative of the Gibbs-Helmholtz equation:

$$\frac{\partial^2 \Delta G_u(T_s)}{\partial^2 T} = -\frac{\Delta C_p}{T_s}$$

for T_s is the temperature where ΔG_u is maximum [2]. A reduction in ΔC_p will make the curvature less negative and, therefore, the protein stability curve is broadened. Similarly, it can be shown that a smaller ΔC_p can increase the maximum ΔG_u: $\Delta G_u(T_s) = \Delta H_m - \Delta C_p(T_m - T_s)$, or in other words, the protein stability curve is up-shifted [2], provided that ΔH_m is increased or remains constant.

Consistent with the observation that most thermophilic proteins achieve higher thermostability by up-shifting and broadening of their protein stability curves, thermophilic proteins tend to have a much smaller value of ΔC_p than their mesophilic homologs [4–11]. For example, we have shown that the thermophilic ribosomal protein L30e from *Thermococcus celer* has a ΔC_p value of ~5 kJ mol^{-1} K^{-1}, which is much smaller than the value of ~10 kJ mol^{-1} K^{-1} obtained for the mesophilic L30e from yeast [12].

In thermophilic proteins, one common strategy to enhance thermostability is to have more favorable surface charge-charge interactions. When compared with their mesophilic homologues, thermophilic proteins have more surface charged residues [13] and have an increased number of salt bridge [14–16]. The

stabilizing role of the electrostatic interaction was first suggested by Perutz and Raidt based on their modeling studies [17,18], and was experimentally verified by various strategies including optimization of surface charges [19,20], removal of surface charges [21,22], addition of new ion pairs [23,24], and double mutant cycles [23,25–34]. To study the contribution of charge-charge interactions to the thermostability and the reduced ΔC_p of thermophilic proteins, our group had systematically removed 26 surface charges on *T. celer* L30e by single charge-to-alanine substitutions. Most of the mutants results in decreases in T_m [21], indicated that the surface charges are mostly stabilizing in thermophilic protein. In another study, we showed that removal of favorable charge-charge interaction by single charge-to-neutral substitutions increases the ΔC_p value [12].

Here, we demonstrated that stabilizing salt-bridges enhance the thermostability of proteins by reducing the ΔC_p. We used the double-mutant cycle to investigate the effect of pair-wise interaction of two salt bridges (E6/R92 and E62/K46) on protein thermostability and ΔC_p. We showed that the two salt-bridges stabilized the *T. celer* L30e protein by ~2–5 kJ mol^{-1}, and the stabilizing effect was insensitive to temperature changes from 298–348 K. The contribution of the two salt-bridges to ΔC_p was determined independently by Gibbs-Helmholtz and Kirchhoff analyses. Our results showed that each salt-bridge contributed to a reduction of ΔC_p by 0.8–1.0 kJ mol^{-1} K^{-1}. That salt-bridge reduces ΔC_p provides a structural basis for the large differences in ΔCp observed between thermophilic and mesophilic proteins.

Results

Design of variants

In this study, we used the double-mutant cycle to investigate how salt-bridges contribute to the thermostability of proteins. We have selected two salt-bridges (E6/R92 and K46/E62), which are located on opposite sides of *T. celer* L30e (Figure 1). Charged residues were substituted with alanine. For Arg and Lys residues that have long side chain, substitutions to Met were made to mimic their long hydrophobic side chains. As a result, two double-mutant cycles were applied for each salt-bridge. As a negative control, we have also used double-mutant cycles to study the pair-wise interaction between E90 and R92, which have a long separation distance of 10.8 Å. A total of seven single mutants and six double mutants were generated (Table S1).

Pair-wise Interaction energy between charge residues was determined by double-mutant cycles

Single charge-to-neutral substitutions suffer from the limitation that the residue being substituted may also form other interactions with the rest of the proteins. By canceling out these interactions using the double-mutant-cycle approach, one can estimate the contribution of the pair-wise interaction between the two oppositely charged residues in a salt-bridge [23]. The scheme presented in Figure S1 explains how the pair-wise interaction energy is determined by the double-mutant-cycle approach. For the theoretical background on the use of double-mutant cycle to determine the pair-wise interaction energy of salt-bridges, please refer to the work of Fersht and co-workers [23]. In brief, if pair-wise interaction exists between two oppositely charged residues, the $\Delta\Delta G_u$ for removing a negative charge from the wild-type protein (process A) should be smaller than that from M^{-ve} in which the positive charged residues has been substituted in prior (process B) (Figure S1). It is because in addition to the interaction made by the negative charge residue to the rest of the protein, the process A also removes the pair-wise interaction. Similar arguments could be applied to the $\Delta\Delta G$ for process C and D. We obtained the pair-wise interaction energy between the two charge residues ($\Delta\Delta G_{int}$) by: $\Delta\Delta G_{int} = [\Delta G_u(DM) - \Delta G_u(M^{-ve})] - [\Delta G_u(M^{+ve}) - \Delta G_u\ (WT)]$.

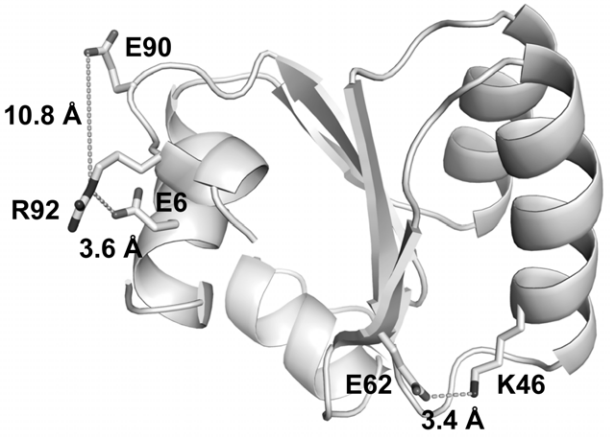

Figure 1. Design of L30e variants. The separation distances of the salt-bridges E6/R92 and E62/K46, and the control pair E90/R92 are indicated and represented by dashed lines.
doi:10.1371/journal.pone.0021624.g001

We have determined the free energy of unfolding (ΔG_u) of the wild-type *T. celer* L30e and its variants by urea-induced denaturation at 298 K (Table 1), and calculated the values $\Delta\Delta G_{int}$ for the cycles E6A/R92A(M), E62A/K46A(M), and E90A/R92A(M) (Figure S1). The values of $\Delta\Delta G_{int}$ were in the range of 1.9–3.6 kJ mol^{-1} for the pairs of charged residues (E6/R92 and E62/K46) involved in salt-bridges. In contrast, the values of $\Delta\Delta G_{int}$ were close to zero for the control pairs (E90/R92). Taken together, our results suggest that the two salt-bridges of E6/R92 and E62/K46 contributed favorably to the stability of L30e.

Table 1. Free energy of unfolding (kJ mol^{-1}) of *T. celer* L30e and its variants at 298–348 K.

Protein	298 K	308 K	318 K	328 K	338 K	348 K
Wild-type	34.9±0.5	35.0±0.5	32.4±0.5	30.8±0.4	26.6±0.4	20.9±0.5
E6A	27.5±0.3	27.7±0.3	25.5±0.3	23.3±0.3	19.0±0.3	14.4±0.3
K46A	29.8±0.3	29.7±0.4	26.7±0.4	24.2±0.3	19.0±0.3	13.3±0.4
K46M	31.1±0.3	30.6±0.4	28.3±0.3	26.3±0.4	22.4±0.3	17.4±0.2
E62A	28.5±0.3	28.7±0.3	25.7±0.3	23.3±0.3	18.0±0.2	12.1±0.3
E90A	32.7±0.4	32.7±0.4	29.8±0.5	29.0±0.4	24.2±0.4	19.8±1.5
R92A	33.9±0.5	33.6±0.5	31.3±0.6	30.8±0.5	25.0±0.4	19.1±0.3
R92M	35.2±0.5	35.4±0.4	32.7±0.4	31.3±0.5	26.0±0.4	19.6±0.3
E6A/R92A	28.4±0.3	28.5±0.4	26.2±0.4	25.1±0.3	19.9±0.3	15.3±0.3
E6A/R92M	29.7±0.3	30.0±0.4	27.7±0.4	26.1±0.3	21.4±0.3	16.0±0.3
E62A/K46A	27.0±0.3	27.0±0.3	24.0±0.3	21.2±0.3	14.5±0.3	8.2±0.5
E62A/K46M	27.8±0.3	27.8±0.3	25.1±0.3	23.2±0.3	18.4±0.2	12.9±0.2
E90A/R92A	32.4±0.4	32.0±0.5	29.7±0.5	29.4±0.5	22.9±0.4	18.3±0.3
E90A/R92M	33.1±0.3	33.3±0.4	30.3±0.4	29.7±0.4	24.7±0.3	19.8±0.3

doi:10.1371/journal.pone.0021624.t001

Salt-bridges are stabilizing and their interaction energies are insensitive to temperature changes

Next we investigated the temperature dependency of the pair-wise interaction energy. The measurement of ΔG_u was extended to 308, 318, 328, 338 and 348 K (Table 1). The values of $\Delta\Delta G_{int}$ were determined accordingly and summarized in Table S2 and Figure S2. Within each double-mutant cycle, there is no significant difference among the $\Delta\Delta G_{int}$ values obtained at different temperatures, and between those derived from R/K→A cycles and from R/K→M cycles. On the other hand, the $\Delta\Delta G_{int}$ values for different pairs of charge residues were significantly different from each other. The average values of $\Delta\Delta G_{int}$ for the salt-bridges E6/R92 and E62/K46 were 2.3±0.3 and 3.9±0.3, respectively, while the value for the control pair was 0.6±0.3 kJ mol^{-1}. Our results suggest that the salt-bridges E6/R92 and E62/K46 are stabilizing, and the pair-wise interaction energy appears to be independent of temperatures.

ΔC_p is reduced by pair-wise interaction of salt-bridges

Values of ΔG_u at temperatures 298–348 K and their T_m values were fitted to the Gibbs-Helmholtz equation to obtain the values of ΔC_p (Figure 2 and Table 2). Compared to the wild-type value of 5.3 kJ mol^{-1} K^{-1}, ΔC_p were increased to 5.7–6.8 kJ mol^{-1} K^{-1} for substitutions (E6A, E62A, K46A/M, R92A/M) that break a salt-bridge interaction. On the other hand, for the E90A substitution that did not break any salt-bridge, there was no significant change in the value of ΔC_p (Table 2). These results suggest that single substitutions that break a salt-bridge would increase the values of ΔC_p.

To address the question if the pair-wise interaction of salt-bridges affects the values of ΔC_p, we determined the $\Delta\Delta C_{p(int)}$ by double-mutant cycle in an analogy to the determination of the $\Delta\Delta G_{int}$ (Figure 3A). Take the double-mutant cycle of E6A/R92A as an example (Figure 3B). Removal of a negative charge by E6A substitution from the wild-type L30e resulted in an increase of ΔC_p for 0.8 kJ mol^{-1} K^{-1}. On the other hand, the difference in ΔC_p between R92A and E6A/R92A was only −0.1 kJ mol^{-1} K^{-1}. These data suggest that the two substitutions are not independent, and the pair-wise interaction between E6A and R92A affects the ΔC_p.

Similar to the argument for the determination of $\Delta\Delta G_{int}$, we have $\Delta\Delta C_{p(int)} = [\Delta C_p(DM) - \Delta C_p(M^{-ve})] - [\Delta C_p(M^{+ve}) - \Delta C_p(WT)]$ (Figure 3A). The values of $\Delta\Delta C_{p(int)}$ for the six double-mutant cycles were determined by the double-mutant cycle (Table 3 and Figure 3B). The values of $\Delta\Delta C_{p(int)}$ for the control cycle, E90A/R92A(M), were close to zero (−0.1 to −0.3 kJ mol^{-1} K^{-1}). In contrast, for the cycles, E6A/R92A(M) and E62A/K46A(M), that involves breakage of a salt-bridge, values of $\Delta\Delta C_{p(int)}$ were from −0.8 to −1.0 kJ mol^{-1} K^{-1}. The negative values of $\Delta\Delta C_{p(int)}$ strongly suggest that the pair-wise interaction of salt-bridges reduces the ΔC_p.

To further confirm the hypothesis that the pair-wise interaction of salt-bridge contributes to the reduction of ΔC_p, we have determined the values of ΔC_p independently by the Kirchhoff analysis [35–37]. Values of T_m and ΔH_m at pH 2.5–6.0 for L30e and its variants were obtained by thermal denaturation. ΔC_p values for wild-type and variant L30e were derived from the slope of the ΔH_m vs. T_m plot (Figure 4), and summarized in Table 2. The ΔC_p value for wild-type L30e was 3.9±0.2 kJ mol^{-1} K^{-1}. For substitutions (E6A, K46A, E62A, R92A) that break a salt-bridge, the ΔC_p values were increased to 4.6–4.9 kJ mol^{-1} K^{-1} (Table 2). On the other hand, for E90A substitution that did not break any salt-bridge, the ΔC_p value was 4.0±0.1 kJ mol^{-1} K^{-1}, which was similar to that of wild-type L30e.

We noticed that ΔC_p values obtained using the Kirchhoff analysis based on thermal denaturation data were smaller than those using Gibbs-Helmholtz analysis based on chemical-induced denaturation experiments. This observation is consistent with our previous report, in which we pointed out that the systematic differences in ΔC_p values were probably due to the thermal denatured state having more residual structures than the chemical-induced denatured state [12].

Regardless of the systematic differences in ΔC_p values, the values of $\Delta\Delta C_{p(int)}$ determined by the Kirchhoff analysis were in striking agreement with those obtained by the Gibbs-Helmholtz analysis (Table 3). For the double-mutant cycles involving the breakage of a salt-bridge, the values of $\Delta\Delta C_{p(int)}$ were −0.8±0.4 and −0.9±0.5 kJ mol^{-1} K^{-1} for E6A/R92A and E62A/K46A, respectively. In contrast, the $\Delta\Delta C_{p(int)}$ was close to zero for the control cycle E90A/R92A (−0.2±0.4 kJ mol^{-1} K^{-1}). Taken together, our results suggest that the pair-wise interaction of salt-bridge reduces the ΔC_p by ca. 0.8–1.0 kJ mol^{-1} K^{-1}.

No major structural changes were observed in the double charge-to-Ala variants

The crystal structures of the E6A/R92A, K46A/E62A, and E90A/R92A variants were determined at resolution ranging from 1.8 to 2.0 Å (Table S3). The structures of all these variants can be superimposable with the wild-type structures (Figure S3). The root-mean-square deviations (r.m.s.d.) between C^{α} atoms of the wild-type L30e and its variants were <0.5 Å (Table S3), suggesting there were no major structural change in these variants.

Discussion

Whether salt-bridge contributes to protein stability is controversial, and is probably context dependent [23,30,38–42]. Elcock proposed that salt-bridge should be more stabilizing at high temperatures because the unfavorable desolvation penalty [43–45] and the entropic cost of fixing two charged side-chains [33,46,47] would decrease with temperatures [48]. Here, we used the double-mutant-cycle approach to study how salt-bridge contributes to the thermostability of proteins. The two salt-bridges, E6/R92 and E62/K46, stabilizes the protein by ~2–5 kJ mol^{-1} (Figure S2 and Table S2). That values of $\Delta\Delta G_{int}$ for R/K→A and R/K→M cycles were similar suggests that the stabilization is mainly due to the charge-charge interaction, rather than hydrophobic interaction, between the salt-bridging residues. We showed that the pair-wise interaction energy, $\Delta\Delta G_{int}$, is insensitive to temperature changes (Figure S2). This observation is consistent with a previous study by Ge and co-workers [26], which showed that the pair-wise interaction energies of salt-bridges in a hyperthermophilic protein Ssh10b at 298 and 353 K were similar. Since the free energy of unfolding is decreasing with temperatures, the more-or-less constant stabilizing effect of salt-bridges should contribute more in proportion to the overall protein stability at high temperatures.

We further demonstrated unambiguously that the stabilizing salt-bridges reduce the heat capacity change of unfolding (ΔC_p). We showed that single-substitutions that break a salt-bridge increased the ΔC_p value. This observation is consistent with our previous report in that removal of favorable electrostatic interactions by single charge-to-neutral substitutions increases the ΔC_p [12]. Using the double-mutant-cycle approach, we determined the values of $\Delta\Delta C_{p(int)}$, which estimates how much the pair-wise interaction between the salt-bridging residues contributes to the heat capacity change of unfolding. For the double-mutant cycles that break a salt-bridge (i.e. E6/R92 and E62/K46),

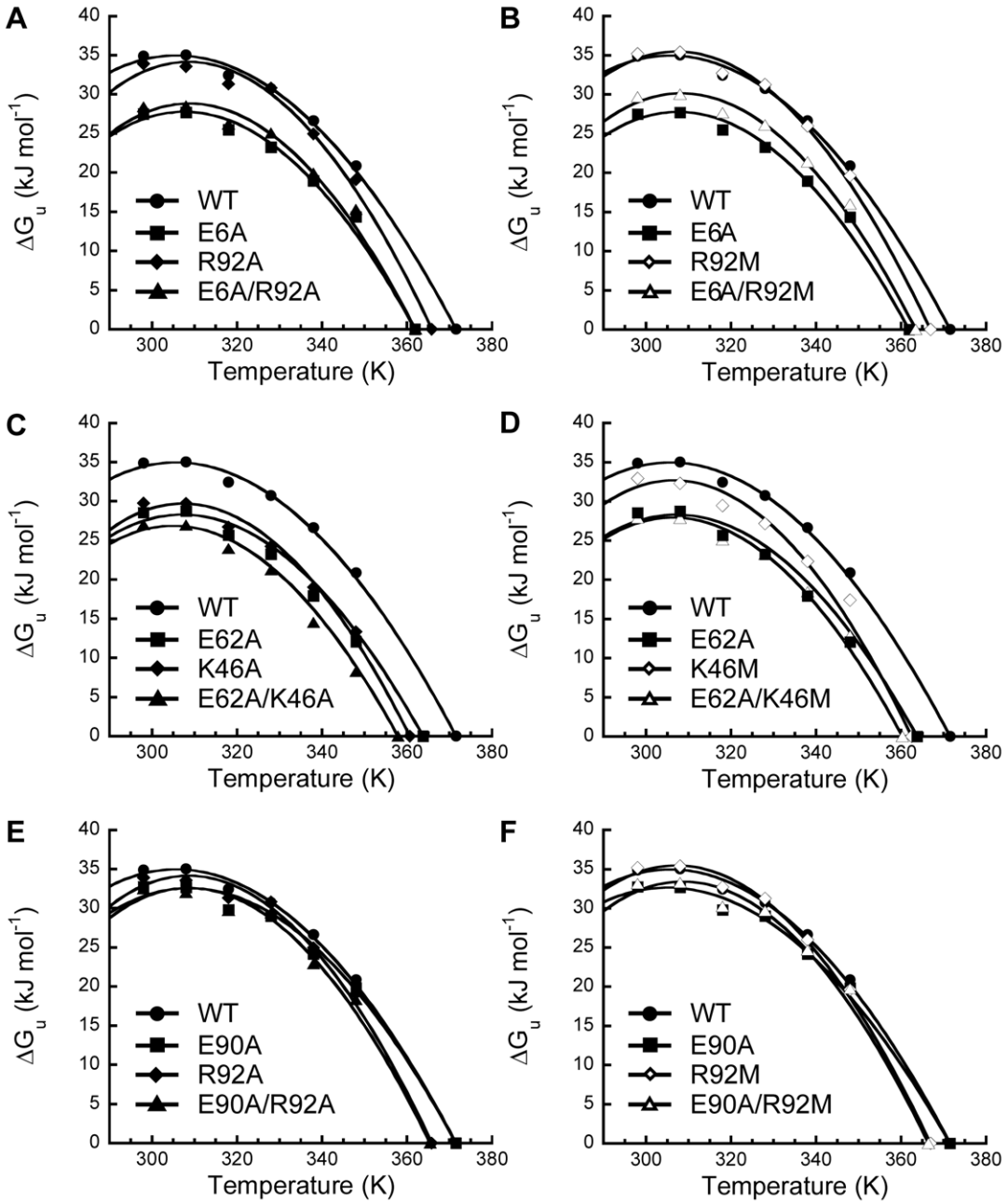

Figure 2. The protein stability curves of *T. celer* L30e and its variants. Values of ΔG_u at 298–348 K were obtained by urea-induced denaturation experiments for the variants of L30e in the double-mutant cycles (A) E6A/R92A, (B) E6A/R92M, (C) E62A/K46A, (D) E62A/K46M, (E) E90A/R92A, and (F) E90A/R92M. Values of ΔG_u for the wild-type L30e are shown in circles, E→A variants in squares, R/K→A/M variants in diamonds, and the doubly-substituted variants in triangles. Values of ΔG_u together with T_m were fitted to the Gibbs-Helmholtz equation to obtain values of ΔC_p.
doi:10.1371/journal.pone.0021624.g002

negative values of $\Delta\Delta C_{p(int)}$ suggest that the pair-wise interaction of the salt-bridges reduces the ΔC_p by 0.8 to 1.0 kJ mol^{-1} K^{-1}.

Using guanidine-induced denaturation and Gibbs-Helmholtz analysis, we have previously showed that the ΔC_p for the mesophilic L30e from yeast (10.5 kJ mol^{-1} K^{-1}) was much larger than that for the thermophilic *T. celer* L30e (5.3 kJ mol^{-1} K^{-1}) [12]. It is in fact a common observation that thermophilic proteins tend to have smaller values of ΔC_p than their mesophilic homologues [4–8,10,11]. Here, we demonstrated by double-mutant cycle that the pair-wise interaction between the salt-bridging residues reduces the ΔC_p, which provide a structural basis of why thermophilic proteins have smaller values of ΔC_p. This conclusion is consistent with our previous observation that removal of favorable charge-charge interactions by single substitutions resulted in increases in ΔC_p [12]. Using a simple spherical model, Zhou predicted that favorable interaction between two oppositely charge residues should decrease ΔC_p [49]. Our experimental results provide unambiguous evidence supporting the conclusion that stabilizing salt-bridge reduces the ΔC_p.

Table 2. ΔC_p (kJ mol^{-1} K^{-1}) of *T. celer* L30e and its variants.

Protein sample	Gibbs-Helmholtz analysis	Kirchhoff analysis
Wild-type	5.3±0.4	3.9±0.2
E6A	6.1±0.3	4.6±0.2
K46A	6.8±0.2	4.8±0.3
K46M	6.8±0.4	ND
E62A	5.7±0.2	4.6±0.2
E90A	5.4±0.2	4.0±0.1
R92A	6.8±0.3	4.9±0.2
R92M	6.5±0.3	ND
E6A/R92A	6.7±0.2	4.8±0.1
E6A/R92M	6.5±0.3	ND
E62A/K46A	6.2±0.2	4.6±0.2
E62A/K46M	6.3±0.3	ND
E90A/R92A	6.6±0.2	4.8±0.2
E90A/R92M	6.5±0.3	ND

doi:10.1371/journal.pone.0021624.t002

The structural basis of why thermophilic proteins have smaller values of ΔC_p is controversial. It has been well documented that ΔC_p correlates well with the changes in solvent accessible surface area (ΔASA) upon unfolding [50–52]. As we have pointed out previously, due to the similarity in their native conformation, homologous proteins tend to bury similar amount of ASA upon folding assuming the denatured states are random coil [12]. To explain the differences in ΔC_p between thermophilic and mesophilic proteins, it has been proposed that thermophilic proteins may have more residual structures in their denatured states so that the ΔASA would be smaller than that calculated for a random-coil [53,54]. However, it is uncertain if the differences in residual structures, if any, can explain the large differences in ΔC_p observed. Moreover, Zhou pointed out that the presence of more residual structures may increase the free energy of the denatured state and destabilize the protein, which is counter-intuitive to the fact that thermophilic proteins are more stable than their mesophilic homologs [49]. Apparently, the correlation of ΔC_p to ΔASA fails to account for the large differences in ΔC_p commonly observed for thermophilic and mesophilic pairs of homologous proteins [8,9], suggesting that factors other than the hydration effect may also contribute to ΔC_p.

Our results showed that the ΔH_m for the wild-type protein was slightly higher than that for the variants (Figure 4). Under this condition, having a smaller ΔC_p always enhances protein thermostability by up-shifting and broadening the protein stability curve. Figure S4 simulates the shape of the protein stability curve of two hypothetical proteins with ΔC_p values of 5.3 and 7.3 kJ mol^{-1} K^{-1}. The simulation shows that a decrease of ΔC_p by 2 kJ mol^{-1} K^{-1} shifts the protein stability upward, and increases its maximum stability by $\sim$10 kJ mol^{-1}. It also broadens the protein stability curve so that the protein remains stable at a wilder range of temperatures. Our previous study also showed *T. celer* L30e has an up-shifted and broadened protein stability curve when compare with that of the mesophilic yeast homologues [12].

In a survey of 26 protein families where thermodynamics data were available for both mesophilic and thermophilic homologs, Razvi and co-workers found that most protein enhances their thermostability by up-shifting and broadening of the protein stability curves [3]. Since thermophilic proteins tend to have more salt-bridges than their mesophilic homologs [14–16], our observation that salt-bridge reduces ΔC_p may provide a general

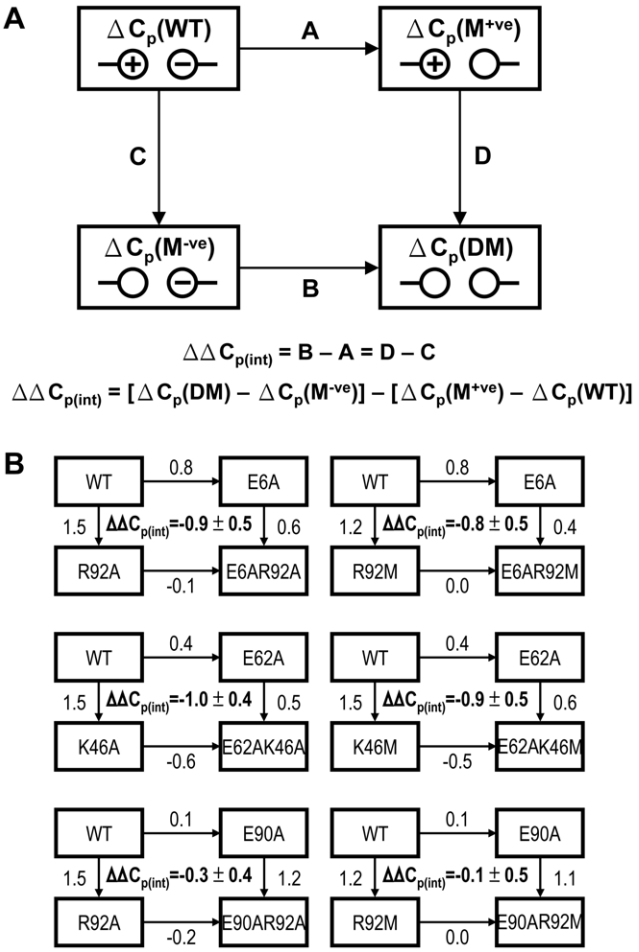

Figure 3. Determination of $\Delta\Delta C_{p(int)}$ by double-mutant cycle analysis. The scheme shown in panel (A) is in analogy to that used to calculate $\Delta\Delta G_{int}$ in Figure S1. (B) $\Delta\Delta C_{p(int)}$ for all six double-mutant cycles analyzed. The substitutions are indicated inside the boxes. The values of $\Delta\Delta C_p$ for processes A–D were shown along the arrows, and the values of $\Delta\Delta C_{p(int)}$ were shown in the middle of the cycles. All values are in kJ mol^{-1} K^{-1}.
doi:10.1371/journal.pone.0021624.g003

Table 3. $\Delta\Delta C_{p(int)}$ (kJ mol^{-1} K^{-1}) determined by double-mutant cycles.

Double-mutant Cycles	Gibbs-Helmholtz analysis	Kirchhoff analysis
E6A/R92A	−0.9±0.6	−0.8±0.4
E6A/R92M	−0.8±0.6	ND
E62A/K46A	−1.0±0.5	−0.9±0.5
E62A/K46M	−0.9±0.7	ND
E90A/R92A	−0.3±0.6	−0.2±0.4
E90A/R92M	−0.1±0.6	ND

doi:10.1371/journal.pone.0021624.t003

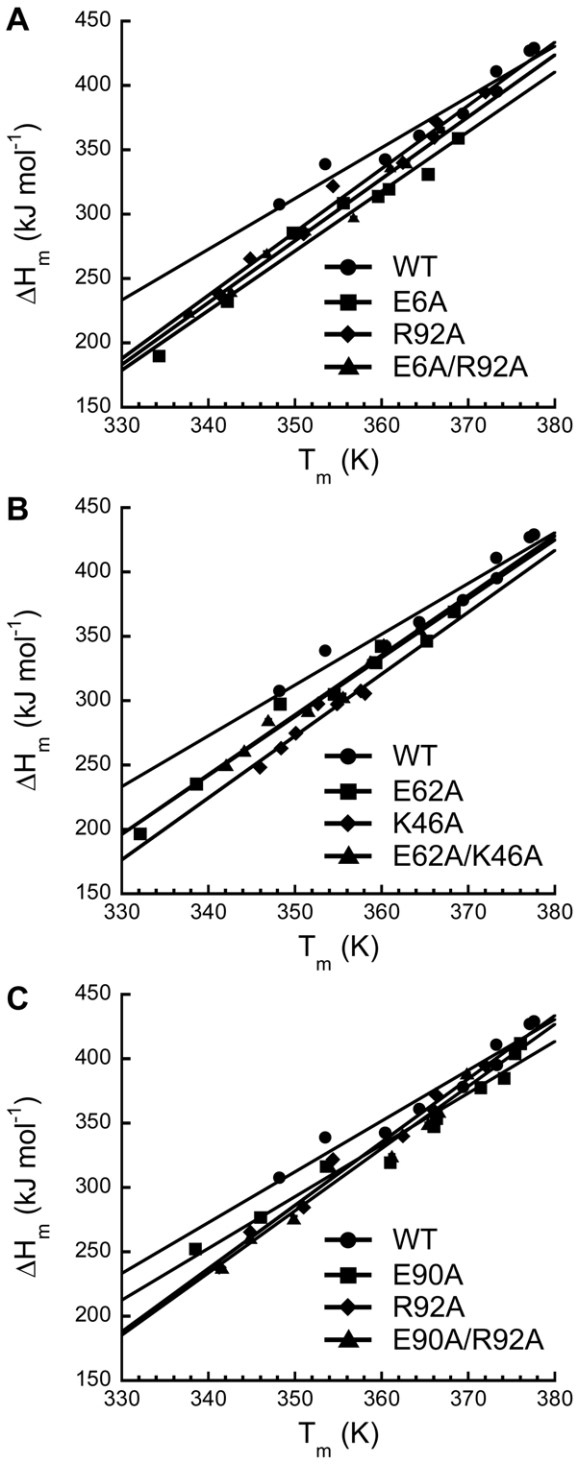

Figure 4. Determination of ΔC_p by the Kirchhoff analysis. ΔH_m and T_m were obtained at pH 2.6–6.0 by thermal denaturation for the variants of L30e in the double-mutant cycles (A) E6A/R92A, (B) E62A/K46A, and (C) E90A/R92A. Values of ΔH_m were plotted as a function of T_m for *T. celer* L30e and its variants. ΔC_p was obtained by the slope of the plot.
doi:10.1371/journal.pone.0021624.g004

mechanism for enhancing thermostability - thermophilic proteins have more stabilizing salt-bridges that reduce the ΔC_p, leading to the up-shifting and broadening of the protein stability curve.

Materials and Methods

Site-directed mutagenesis

All site-directed mutagenesis were performed by a two-stage PCR procedure modified from the QuikChange site-directed mutagenesis protocol using the mutagenic primers listed in Table S1 [55]. Wild-type *T. celer* L30e cloned in expression vector pET3d (Novagen) was used as the template in all polymerase reactions. Mutations introduced were confirmed by DNA sequencing.

Protein expression and purification

All protein samples were expressed and purified as described [21,56].

Thermal-induced denaturation

20 μM protein samples were dialyzed in 10 mM sodium acetate buffer at pH 5.4 for 16 hours before circular dichroism (CD) measurement. After degassing thoroughly, all protein samples were heated in a securely stoppered 1 mm path-length cuvette from 298 K to 383 K at a heating rate of 1 K min^{-1}. The thermal denaturation was then monitored by molar ellipticity at 222 nm using a JASCO J810 spectropolarimeter equipped with a peltier-type temperature control unit.

The melting temperature (T_m) and enthalpy of unfolding ΔH_m were obtained by fitting the thermal denaturation curve to a two-state model (Figure S5):

$$y_{obs} = \frac{(y_n + m_n T) + (y_u + m_u T) e^{-\Delta H_m / R(1/T - 1/T_m)}}{1 + e^{-\Delta H_m / R(1/T - 1/T_m)}}$$

where y_{obs} is the observed molar ellipticity at 222 nm; y_n and m_n are the y-intercept and slope of the pre-transition baseline; y_u and m_u are the y-intercept and slope of the post-transition baseline; R is the gas constant; T is the temperature in Kelvin.

Urea-induced denaturation

20 μM protein samples were equilibrated with 0 M–10.2 M urea in 10 mM sodium acetate buffer at pH 5.4 for 30 minutes before CD measurement. Concentration of urea was determined from refractive index measurements [57] using Leica AR200 refractometer. The urea-induced denaturation was monitored by molar ellipticity at 222 nm using a JASCO J810 spectropolarimeter equipped with a peltier-type temperature control unit. The urea-induced denaturation was analyzed by a two-state model [58] (Figure S6):

$$y_{obs} = \frac{(y_n + m_n[D]) + (y_u + m_u[D]) e^{-\Delta G_{(D)} / RT}}{1 + e^{-\Delta G_{(D)} / RT}}$$

where y_{obs} is the observed molar ellipticity at 222 nm; y_n and m_n are the y-intercept and slope of the pre-transition baseline; y_u and m_u are the y-intercept and slope of the post-transition baseline; R is the gas constant; T is the temperature in Kelvin; [D] is the concentration of urea; $\Delta G_{(D)}$ is the free energy change of unfolding at [D]. The free energy change of unfolding without denaturant, ΔG_u, was obtained by linear extrapolation model [58]: $\Delta G_{(D)} = \Delta G_u - m[D]$, using the average m-value approach [59]. ΔG_u at 298 K, 308 K, 318 K, 328 K, 338 K, and 348 K were measured for *T. celer* L30e and its mutants.

Estimation of ΔC_p by Gibbs-Helmholtz analysis

ΔG_u at temperatures from 298 K to 348 K and T_m were fitted to the Gibbs-Helmholtz equation to obtain the values of ΔC_p. For

variants of L30e (E6A, K46M, E6AR92A, and E6AR92M) that exhibited irreversible thermal denaturation, values of apparent T_m were used. The program PRISM (GraphPad Software, La Jolla, USA) was used to estimate the errors in ΔC_p due to the uncertainty in ΔG_u.

Estimation of ΔC_p by Kirchhoff analysis

Thermal-induced denaturation curves were measured for protein samples of *T. celer* L30e in 10 mM sodium citrate/phosphate buffer at pH 2.5 to 6.0. T_m and ΔH_m were obtained from by fitting the data to the two-state model described above. ΔC_p values were then obtained from the slope of the ΔH_m vs. T_m plot. Only the data obtained from reversible thermal denaturation were included in the Kirchhoff analysis.

Crystal structure determination

Crystals of L30e variants were grown by sitting-drop-vapor-diffusion method at 289 K. 2 µl of 10 mg ml^{-1} protein sample was mixed with 2 µl of precipitant solution (Table S3). Datasets were acquired and collected at 100 K using an in-house rotating anode X-ray source. The diffraction data were processed, merged, scaled, and reduced with programs (MOSFLM, SCALA, TRUNCATE) from the CCP4 suite [60]. The structures were solved by molecular replacement using PHENIX with the wild-type *T. celer* L30e crystal structure (PDB code: 1H7M) as the search model. The structures were refined using PHENIX [61], and were validated using WHATCHECK [62] and MOLPROBITY [63,64].

Supporting Information

Figure S1 Coupling energies ($\Delta\Delta G_{int}$) were determined by double-mutant cycles. (A) The scheme explaining how $\Delta\Delta G_{int}$ are calculated from values of ΔG_u for wild-type (WT), single-mutants (M^{+ve} and M^{-ve}), and double-mutant (DM) by the double-mutant cycle analysis. (B) $\Delta\Delta G_{int}$ for all six double-mutant cycles analyzed. The substitutions are indicated inside the boxes. The values of $\Delta\Delta G_u$ for processes A–D were shown along the arrows, and the values of $\Delta\Delta G_{int}$ were shown in the middle of the cycles. All values are in kJ mol^{-1}.
(PDF)

Figure S2 Temperature dependency of the coupling energy. Values of $\Delta\Delta G_{int}$ derived from double-mutant cycles (A) E6A/R92A(M) (circles), (B) E62A/K46A(M) (squares), and (C) E90A/R92A(M) (diamonds) at temperatures 298 K to 348 K are shown. Values of $\Delta\Delta G_{int}$ derived from the R/K→A cycles are represented by filled symbols, and those from the R/K→M cycles by open symbols.
(PDF)

Figure S3 Crystal structures of variants of *T. celer* L30e. Crystal structures of E6A/R92A (red), E62A/K46A (green), and E90A/R92A (blue) are superimposable to the wild-type *T. celer* L30e (black).
(PDF)

Figure S4 Reduced ΔC_p up-shifts and broadens the protein stability curve. The protein stability curve of a hypothetical protein with $\Delta C_p = 7.3$ kJ mol^{-1} K^{-1}, $T_m = 356$ K, $\Delta H_m = 382$ kJ mol^{-1} was simulated using the Gibbs-Helmholtz equation (dashed line). Keeping ΔH_m and T_s (temperature for maximum stability) constant, the protein stability curve with a reduced value of $\Delta C_p = 5.3$ kJ mol^{-1} K^{-1} was simulated as the solid line.
(PDF)

Figure S5 Thermal denaturation of wild-type *T. celer* L30e at different pH. The thermal denaturation curves of wild-type *T. celer* L30e in 10 mM citrate/phosphate buffer at pH ranging from 2.5 to 6.0 were shown.
(PDF)

Figure S6 Urea-induced denaturation of wild-type *T. celer* L30e at different temperatures. The 52-point urea-induced denaturation curves of wild-type *T. celer* L30e in 10 mM sodium acetate buffer, pH 5.4 at temperatures ranging from 298 K to 348 K were shown.
(PDF)

Table S1 Oligonucleotide primers used in the mutagenesis.
(DOC)

Table S2 $\Delta\Delta G_{int}$ at 298–348 K determined by double-mutant cycles.
(DOC)

Table S3 Statistics for crystal structure determination of E6A/R92A, E62A/K46A, E90A/R92A.
(DOC)

Author Contributions

Conceived and designed the experiments: C-HC K-BW. Performed the experiments: C-HC T-HY. Analyzed the data: C-HC T-HY K-BW. Contributed reagents/materials/analysis tools: K-BW. Wrote the paper: C-HC K-BW.

References

1. Nojima H, Ikai A, Oshima T, Noda H (1977) Reversible thermal unfolding of thermostable phosphoglycerate kinase. J Mol Biol 116: 429–442.
2. Kumar S, Tsai CJ, Nussinov R (2001) Thermodynamic differences among homologous thermophilic and mesophilic proteins. Biochemistry 40: 14152–14165.
3. Razvi A, Scholtz JM (2006) Lessons in stability from thermophilic proteins. Protein Sci 15: 1569–1578.
4. Beadle BM, Baase WA, Wilson DB, Gilkes NR, Shoichet BK (1999) Comparing the thermodynamic stabilities of a related thermophilic and mesophilic enzyme. Biochemistry 38: 2570–2576.
5. Deutschman WA, Dahlquist FW (2001) Thermodynamic basis for the increased thermostability of CheY from the hyperthermophile Thermotoga maritima. Biochemistry 40: 13107–13113.
6. Filimonov VV, Azuaga AI, Viguera AR, Serrano L, Mateo PL (1999) A thermodynamic analysis of a family of small globular proteins: SH3 domains. Biophys Chem 77: 195–208.
7. Grattinger M, Dankesreiter A, Schurig H, Jaenicke R (1998) Recombinant phosphoglycerate kinase from the hyperthermophilic bacterium Thermotoga maritima: catalytic, spectral and thermodynamic properties. J Mol Biol 280: 525–533.
8. Hollien J, Marqusee S (1999) A thermodynamic comparison of mesophilic and thermophilic ribonucleases H. Biochemistry 38: 3831–3836.
9. Motono C, Oshima T, Yamagishi A (2001) High thermal stability of 3-isopropylmalate dehydrogenase from Thermus thermophilus resulting from low DeltaC(p) of unfolding. Protein Eng 14: 961–966.
10. Nojima H, Ikai A, Oshima T, Noda H (1977) Reversible thermal unfolding of thermostable phosphoglycerate kinase. Thermostability associated with mean zero enthalpy change. J Mol Biol 116: 429–442.
11. Uchiyama S, Hasegawa J, Tanimoto Y, Moriguchi H, Mizutani M, et al. (2002) Thermodynamic characterization of variants of mesophilic cytochrome c and its thermophilic counterpart. Protein Eng 15: 455–462.
12. Lee CF, Allen MD, Bycroft M, Wong KB (2005) Electrostatic interactions contribute to reduced heat capacity change of unfolding in a thermophilic ribosomal protein l30e. J Mol Biol 348: 419–431.
13. Fukuchi S, Nishikawa K (2001) Protein surface amino acid compositions distinctively differ between thermophilic and mesophilic bacteria. J Mol Biol 309: 835–843.
14. Kumar S, Tsai CJ, Nussinov R (2000) Factors enhancing protein thermostability. Protein Eng 13: 179–191.

15. Szilagyi A, Zavodszky P (2000) Structural differences between mesophilic, moderately thermophilic and extremely thermophilic protein subunits: results of a comprehensive survey. Structure 8: 493–504.
16. Vogt G, Argos P (1997) Protein thermal stability: hydrogen bonds or internal packing? Fold Des 2: S40–46.
17. Perutz MF (1978) Electrostatic effects in proteins. Science 201: 1187–1191.
18. Perutz MF, Raidt H (1975) Stereochemical basis of heat stability in bacterial ferredoxins and in haemoglobin A2. Nature 255: 256–259.
19. Gribenko AV, Patel MM, Liu J, McCallum SA, Wang C, et al. (2009) Rational stabilization of enzymes by computational redesign of surface charge-charge interactions. Proc Natl Acad Sci U S A 106: 2601–2606.
20. Schweiker KL, Zarrine-Afsar A, Davidson AR, Makhatadze GI (2007) Computational design of the Fyn SH3 domain with increased stability through optimization of surface charge charge interactions. Protein Sci 16: 2694–2702.
21. Lee CF, Makhatadze GI, Wong KB (2005) Effects of charge-to-alanine substitutions on the stability of ribosomal protein L30e from Thermococcus celer. Biochemistry 44: 16817–16825.
22. Takano K, Tsuchimori K, Yamagata Y, Yutani K (2000) Contribution of salt bridges near the surface of a protein to the conformational stability. Biochemistry 39: 12375–12381.
23. Serrano L, Horovitz A, Avron B, Bycroft M, Fersht AR (1990) Estimating the contribution of engineered surface electrostatic interactions to protein stability by using double-mutant cycles. Biochemistry 29: 9343–9352.
24. Vetriani C, Maeder DL, Tolliday N, Yip KS, Stillman TJ, et al. (1998) Protein thermostability above 100 degreesC: a key role for ionic interactions. Proc Natl Acad Sci U S A 95: 12300–12305.
25. Blasie CA, Berg JM (1997) Electrostatic interactions across a beta-sheet. Biochemistry 36: 6218–6222.
26. Ge M, Xia XY, Pan XM (2008) Salt bridges in the hyperthermophilic protein Ssh10b are resilient to temperature increases. J Biol Chem 283: 31690–31696.
27. Ibarra-Molero B, Zitzewitz JA, Matthews CR (2004) Salt-bridges can stabilize but do not accelerate the folding of the homodimeric coiled-coil peptide GCN4-p1. J Mol Biol 336: 989–996.
28. Lassila KS, Datta D, Mayo SL (2002) Evaluation of the energetic contribution of an ionic network to beta-sheet stability. Protein Sci 11: 688–690.
29. Luisi DL, Snow CD, Lin JJ, Hendsch ZS, Tidor B, et al. (2003) Surface salt bridges, double-mutant cycles, and protein stability: an experimental and computational analysis of the interaction of the Asp 23 side chain with the N-terminus of the N-terminal domain of the ribosomal protein l9. Biochemistry 42: 7050–7060.
30. Makhatadze GI, Loladze VV, Ermolenko DN, Chen X, Thomas ST (2003) Contribution of surface salt bridges to protein stability: guidelines for protein engineering. J Mol Biol 327: 1135–1148.
31. Marqusee S, Sauer RT (1994) Contributions of a hydrogen bond/salt bridge network to the stability of secondary and tertiary structure in lambda repressor. Protein Sci 3: 2217–2225.
32. Spek EJ, Bui AH, Lu M, Kallenbach NR (1998) Surface salt bridges stabilize the GCN4 leucine zipper. Protein Sci 7: 2431–2437.
33. Strop P, Mayo SL (2000) Contribution of surface salt bridges to protein stability. Biochemistry 39: 1251–1255.
34. Tissot AC, Vuilleumier S, Fersht AR (1996) Importance of two buried salt bridges in the stability and folding pathway of barnase. Biochemistry 35: 6786–6794.
35. Baldwin RL (1986) Temperature dependence of the hydrophobic interaction in protein folding. Proc Natl Acad Sci U S A 83: 8069–8072.
36. Murphy KP, Privalov PL, Gill SJ (1990) Common features of protein unfolding and dissolution of hydrophobic compounds. Science 247: 559–561.
37. Privalov PL, Gill SJ (1988) Stability of protein structure and hydrophobic interaction. Adv Protein Chem 39: 191–234.
38. Erwin CR, Barnett BL, Oliver JD, Sullivan JF (1990) Effects of engineered salt bridges on the stability of subtilisin BPN'. Protein Eng 4: 87–97.
39. Horovitz A, Serrano L, Avron B, Bycroft M, Fersht AR (1990) Strength and co-operativity of contributions of surface salt bridges to protein stability. J Mol Biol 216: 1031–1044.
40. Lam SY, Yeung RC, Yu TH, Sze KH, Wong KB (2011) A rigidifying salt-bridge favors the activity of thermophilic enzyme at high temperatures at the expense of low-temperature activity. PLoS Biol 9: e1001027.
41. Sali D, Bycroft M, Fersht AR (1991) Surface electrostatic interactions contribute little of stability of barnase. J Mol Biol 220: 779–788.
42. Sun DP, Sauer U, Nicholson H, Matthews BW (1991) Contributions of engineered surface salt bridges to the stability of T4 lysozyme determined by directed mutagenesis. Biochemistry 30: 7142–7153.
43. Fersht AR, Serrano L (1993) Principles of protein stability derived from protein engineering experiments. Current Opinion in Structural Biology 3: 75–83.
44. Hendsch ZS, Tidor B (1994) Do salt bridges stabilize proteins? A continuum electrostatic analysis. Protein Sci 3: 211–226.
45. Matthews BW (1993) Structural and genetic analysis of protein stability. Annu Rev Biochem 62: 139–160.
46. Hendsch ZS, Jonsson T, Sauer RT, Tidor B (1996) Protein stabilization by removal of unsatisfied polar groups: computational approaches and experimental tests. Biochemistry 35: 7621–7625.
47. Waldburger CD, Schildbach JF, Sauer RT (1995) Are buried salt bridges important for protein stability and conformational specificity? Nat Struct Biol 2: 122–128.
48. Elcock AH (1998) The stability of salt bridges at high temperatures: implications for hyperthermophilic proteins. J Mol Biol 284: 489–502.
49. Zhou HX (2002) Toward the physical basis of thermophilic proteins: linking of enriched polar interactions and reduced heat capacity of unfolding. Biophys J 83: 3126–3133.
50. Murphy KP, Freire E (1992) Thermodynamics of structural stability and cooperative folding behavior in proteins. Adv Protein Chem 43: 313–361.
51. Myers JK, Pace CN, Scholtz JM (1995) Denaturant m values and heat capacity changes: relation to changes in accessible surface areas of protein unfolding. Protein Sci 4: 2138–2148.
52. Spolar RS, Livingstone JR, Record MT, Jr. (1992) Use of liquid hydrocarbon and amide transfer data to estimate contributions to thermodynamic functions of protein folding from the removal of nonpolar and polar surface from water. Biochemistry 31: 3947–3955.
53. Robic S, Berger JM, Marqusee S (2002) Contributions of folding cores to the thermostabilities of two ribonucleases H. Protein Sci 11: 381–389.
54. Robic S, Guzman-Casado M, Sanchez-Ruiz JM, Marqusee S (2003) Role of residual structure in the unfolded state of a thermophilic protein. Proc Natl Acad Sci U S A 100: 11345–11349.
55. Wang W, Malcolm BA (1999) Two-stage PCR protocol allowing introduction of multiple mutations, deletions and insertions using QuikChange Site-Directed Mutagenesis. Biotechniques 26: 680–682.
56. Wong KB, Lee CF, Chan SH, Leung TY, Chen YW, et al. (2003) Solution structure and thermal stability of ribosomal protein L30e from hyperthermophilic archaeon Thermococcus celer. Protein Sci 12: 1483–1495.
57. Pace CN (1986) Determination and analysis of urea and guanidine hydrochloride denaturation curves. Methods Enzymol 131: 266–280.
58. Santoro MM, Bolen DW (1988) Unfolding free energy changes determined by the linear extrapolation method. 1. Unfolding of phenylmethanesulfonyl alpha-chymotrypsin using different denaturants. Biochemistry 27: 8063–8068.
59. Itzhaki LS, Otzen DE, Fersht AR (1995) The structure of the transition state for folding of chymotrypsin inhibitor 2 analysed by protein engineering methods: evidence for a nucleation-condensation mechanism for protein folding. J Mol Biol 254: 260–288.
60. Collaborative Computational Project N (1994) The CCP4 suite: programs for protein crystallography. Acta Crystallogr D Biol Crystallogr 50: 760–763.
61. Adams PD, Afonine PV, Bunkoczi G, Chen VB, Davis IW, et al. (2010) PHENIX: a comprehensive Python-based system for macromolecular structure solution. Acta Crystallogr D Biol Crystallogr 66: 213–221.
62. Hooft RW, Vriend G, Sander C, Abola EE (1996) Errors in protein structures. Nature 381: 272.
63. Chen VB, Arendall WB, 3rd, Headd JJ, Keedy DA, Immormino RM, et al. (2010) MolProbity: all-atom structure validation for macromolecular crystallography. Acta Crystallogr D Biol Crystallogr 66: 12–21.
64. Davis IW, Leaver-Fay A, Chen VB, Block JN, Kapral GJ, et al. (2007) MolProbity: all-atom contacts and structure validation for proteins and nucleic acids. Nucleic Acids Res 35: W375–383.